JOC The Journal of Organic Chemistry

Note

pubs.acs.org/joc

Fluorescent Peptoids as Selective Live Cell Imaging Probes

Saulo T. A. Passos,[†] José R. Correa,[‡] Samira L. M. Soares,[‡] Wender A. da Silva,*[,†] and Brenno A. D. Neto*[,‡]

[†]Laboratory of Bioactive Compounds Synthesis N.T.S., University of Brasilia (IQ-UnB), Campus Universitário Darcy Ribeiro, Brasília, DF, Brazil

[‡]Laboratory of Medicinal and Technological Chemistry, University of Brasília, Chemistry Institute (IQ-UnB), Campus Universitário Darcy Ribeiro, CEP 70904-970, P.O. Box 4478, Brasília, DF, Brazil

Supporting Information

ABSTRACT: This paper describes the synthesis of fluorescent peptoids using the Ugi multicomponent reaction (4CR). The four synthesized structures had their photophysical properties evaluated and their potential as biomarkers established. The peptidomimetics were used at very low concentrations (10 nM) to follow their internalization in breast cancer cells and had their localization precisely determined. One of the new peptoids displayed mitochondrial affinity and stained this important organelle selectively. Co-staining experiments using MitoTracker Red confirmed the localization inside live cells.

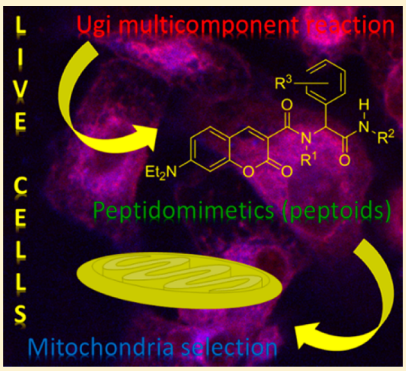

Peptidomimetics like peptoids are synthetic alternatives to the use of naturally occurring peptides. Natural peptides suffer from drawbacks such as proteolysis reactions and, in many cases, a lack of bioavailability. Peptoids are in this sense promising candidates for the replacement of many peptides, especially considering their capability of mimicking biologically relevant secondary protein structures.[1] The possibility of incorporating a myriad of functional groups or substituents on the peptoid structures also fosters interest in the synthesis and biological application of these derivatives. The Ugi four-component (multicomponent) reaction (U4CR) is an outstanding tool for straight access to new peptoid libraries.[2] Some synthetic peptoids obtained by the U4CR have been used as photoaffinity scaffolds linked to small molecule probes,[3] such as a pH-sensitive probe,[4] cyclic peptide analogues,[5] and others.[6−8]

Among some drawbacks to further the use of peptoid derivatives, the lack of information about their subcellular localization is hindering both a rational design and further biological application of these derivatives. It has been described that small chemical modifications afford Ugi adducts with a huge biological behavior difference, therefore suggesting the need for empirically guided optimization.[3] The knowledge of a precise subcellular localization has been described as a prime consideration in the design of new bioactive compounds for cellular studies.[9] With the aim being cellular studies, the molecule must be capable of transposing the cell membrane[10] and selectively targeting a specific organelle or cell component.[11]

The elegant synthetic strategy for incorporating fluorescent tags into a promising bioactive compound allows us in principle to follow their dynamics and to determine their precise subcellular localization inside (live) cells, as we have recently highlighted.[12] Because of our interest in the U4CR[13] (and multicomponent reactions[14−19]) and bioprobes as selective live cell fluorescence imaging probes,[20−23] we disclose herein our findings after the incorporation of a fluorescent coumarin[24−26] tag into four new peptoids synthesized using the U4CR applied for live cell imaging experiments.

The new peptidomimetics (named **P1−P4**) were synthesized using the well-established Ugi reaction (Scheme 1). After the structures had been characterized, **P1−P4** were used at a nanomolar concentration (very low concentration) to avoid any interference with cellular homeostasis, aiming at disclosing whether the new structures could transpose the cells' membranes and at verifying any specific interaction (cellular selectivity) inside the live cancer cells.

All compounds were obtained as expected and had their photophysical properties determined (Figure S1 of the Supporting Information). Table 1 summarizes the photophysical properties measured for **P1−P4**.

All compounds showed good stability in the excited state and reasonable Stokes shifts. Large molar extinction coefficients were observed for all compounds (log ε of ∼4.00). Figure S1 shows the standard photophysical data measured for the new peptidomimetics. All R^2 values obtained for the microscopic solvent polarity parameters (E_T^N)[27] in the solvatochromic method[28] plots are close to (but above) 0.60 (Figure S1),

Received: January 6, 2016
Published: February 17, 2016

DOI: 10.1021/acs.joc.6b00034
J. Org. Chem. 2016, 81, 2646−2651

Scheme 1. Synthesis of the New Fluorescent Peptoids P1−P4 through the Ugi Reaction[a]

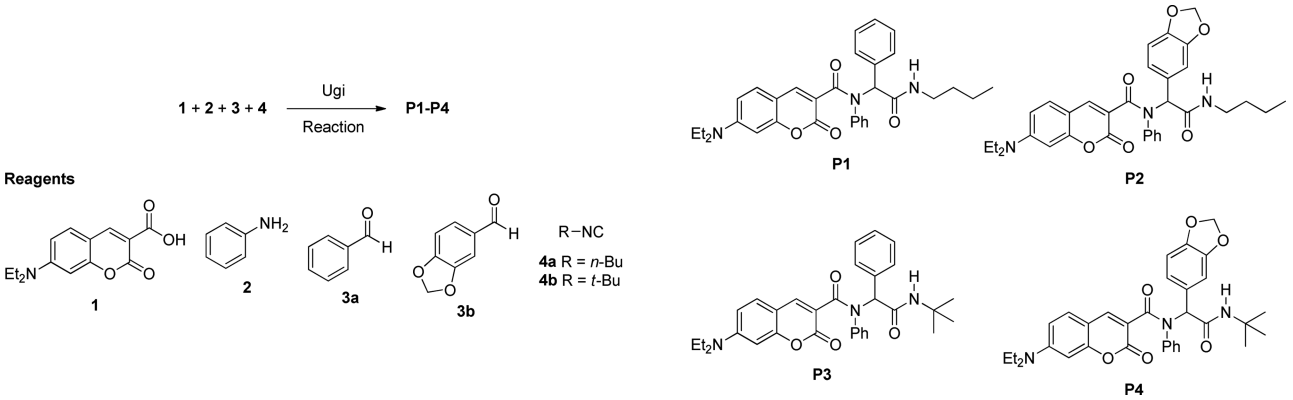

[a]Note the incorporation of a fluorescent tag (coumarin derivative **1**) in all structures.

Table 1. Photophysical Data (in different solvents) for P1−P4

peptoid[a]	solvent	λ_{max}(abs) (nm)	log ε (ε)	λ_{max}(em) (nm)	Stokes shift (nm)
P1	ethyl acetate	397	4.00 (10050)	455	58
	acetonitrile	405	3.96 (9070)	465	60
	chloroform	411	3.71 (5170)	453	42
	dichloromethane	412	3.89 (7820)	460	48
	ethanol	405	3.80 (6260)	465	60
	hexane	388	4.3544 (22620)	418	30
	methanol	407	3.86 (7170)	469	67
	toluene	399	3.79 (6180)	441	42
	water	424	3.74 (5500)	473	49
P2	ethyl acetate	396	3.69 (4960)	453	57
	acetonitrile	403	3.96 (9020)	464	61
	chloroform	411	3.48 (3041)	454	43
	dichloromethane	410	4.17 (14840)	460	50
	ethanol	405	3.90 (7988)	467	62
	hexane	388	4.14 (13670)	417	29
	methanol	407	3.91 (8150)	472	65
	toluene	400	3.73 (5350)	444	44
	water	428	3.17 (1470)	474	46
P3	ethyl acetate	396	4.55 (35880)	455	59
	acetonitrile	405	3.99 (9900)	464	59
	chloroform	408	4.37 (23640)	452	44
	dichloromethane	409	4.37 (23670)	459	50
	ethanol	404	4.06 (11460)	467	63
	hexane	388	3.76 (5750)	418	30
	methanol	406	4.53 (33840)	470	64
	toluene	399	4.38 (23830)	444	45
	water	425	3.43 (2700)	471	46
P4	ethyl acetate	396	4.67 (46910)	453	57
	acetonitrile	405	4.70 (49690)	467	62
	chloroform	407	4.56 (36570)	454	47
	dichloromethane	409	4.74 (54660)	457	48
	ethanol	404	4.36 (22990)	465	61
	hexane	388	4.64 (43560)	418	30
	methanol	406	4.63 (43080)	470	64
	toluene	398	4.46 (28980)	445	47
	water	423	3.26 (1800)	484	61

[a]Quantum yields for **P1−P4** of 0.20, 0.27, 0.12, and 0.67, respectively.

therefore indicating ICT stabilization from the excited state and the difference in the polarity of the structures when comparing ground and excited states. Photostability experiments (Figure S2) under constant UV irradiation (365 nm) were also performed, and **P1−P4** could sustain their fluorescence intensity for at least 2 h with no notable decrease in their emission.

P1−P4 were therefore subjected to cellular experiments using the MCF-7 (human breast adenocarcinoma) cell lineage (live and fixed samples). One major challenge of bioimaging

DOI: 10.1021/acs.joc.6b00034
J. Org. Chem. 2016, 81, 2646−2651

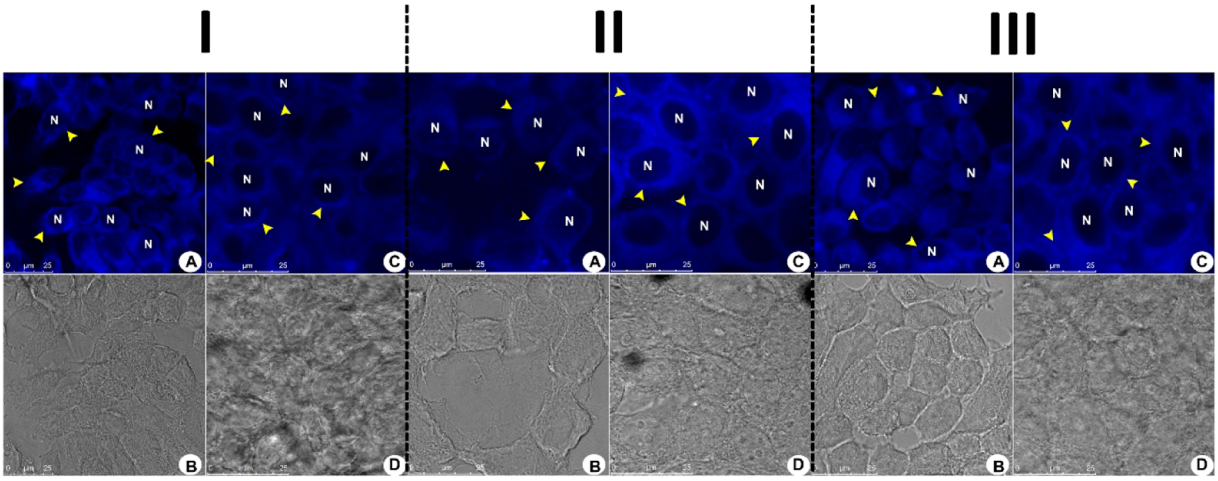

Figure 1. Fluorescence profile of MCF-7 cells incubated with **P1**−**P3** (10 nM, blue emission). (I) Peptoid **P1**, (II) Peptoid **P2**, and (III) Peptoid **P3**. Panels A and C show live and fixed cell samples, respectively. Panels B and D show the normal morphological aspects of the samples by phase contrast microscopy. Yellow arrows show the fluorescent staining pattern (blue) that slightly spread through the cell cytoplasm with accumulation near the cells' nuclei. No fluorescent signal could be detected inside of the nuclei of the cells (N). Reference scale bar of 25 μm.

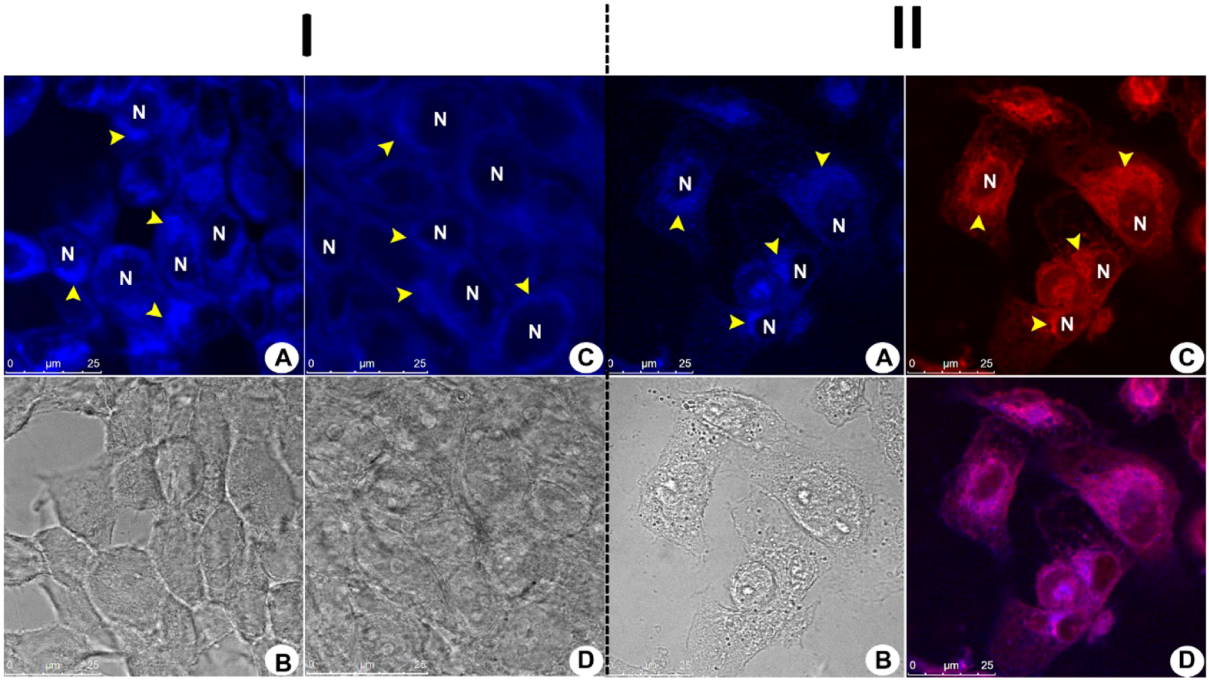

Figure 2. Fluorescence profile of MCF-7 cells incubated with **P4** (10 nM, blue emission). (I) Panels A and C show live and fixed cell samples, respectively. Panels B and D show the normal morphological aspects of the samples by phase contrast microscopy. Yellow arrows show the fluorescent staining pattern (blue), which was concentrated in a restricted cellular region near the cells' nuclei, that is, concentrated at the mitochondria. No fluorescent signal could be detected inside of cellular nuclei (N). (II) Fluorescent profiles of MCF-7 cells incubated with peptoid **P4** and commercially available MitoTracker Red. Panels A and C show fluorescence patterns from cells incubated with peptoid **P4** and commercially available MitoTracker Red, respectively. The yellow arrows indicate the cytoplasm accumulation region of the same cells for both markers. (D) Panel produced by the overlay (purple) of the blue (**P4**) and red (MitoTracker Red) fluorescence images from panels A and C to prove the accumulation of **P4** at the mitochondria. (B) Morphological aspects of the samples by phase contrast microscopy. The cells' nuclei are shown as black voids identified by the letter "N". Reference scale bar of 25 μm.

experiments is to use low concentrations of the tested peptoids to avoid any cytotoxic effect. This is an important feature to really aid in the collection of information regarding the internalization processes and dynamics; otherwise, the peptoids could induce cell death or changes in the cells' morphological structures, thus avoiding a precise study of their subcellular localization, which is in turn of paramount importance for depicting their cellular action. Peptoids typically display a cytotoxic effect up to micromolar concentrations, as recently shown for some derivatives.[29−31] In this context, we have conducted the cell viability (MTT assays) experiments (Figure S3) using nanomolar concentrations (100 nM).

As depicted from Figure S3 (at low concentrations, 100 nM), the synthesized peptoids showed no cytotoxic effect hence validated for bioimaging assays at low concentrations. All cell imaging experiments were conducted using only a concen-

DOI: 10.1021/acs.joc.6b00034
J. Org. Chem. 2016, 81, 2646−2651

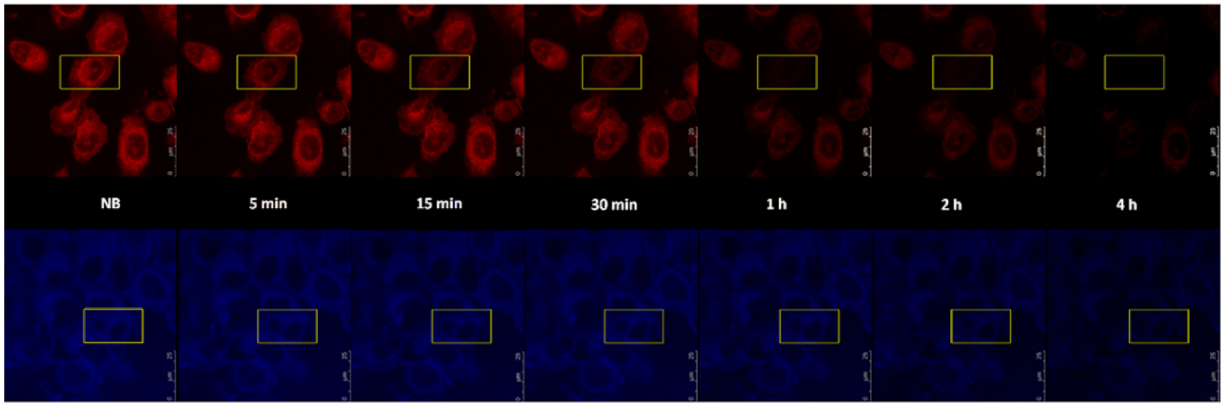

Figure 3. **P4** and MitoTracker Red fluorescence emissions after photobleaching. The yellow rectangles are the regions of interest (ROI) delimitation, and they have all the same area. No accentuate fading off in the fluorescence emission from **P4** stain could be visually noted during the experimental time period. Note that samples were not subjected to photobleaching. Reference scale bar of 25 μm.

tration for the peptidomimetics of ∼10 nM, that is, a concentration 10-fold lower than that used for the MTT assays (Figure S3), to ensure no interference in the cellular processes or morphological alterations of the cells aiming at a precise subcellular localization and to depict their distribution (dynamics). No photobleaching could be visually noted during the experiment time period for all tested molecules.

Peptoids **P1**−**P4** were then subjected to cell imaging experiments. **P1**−**P3** showed interesting results (Figure 1) but with no actual cellular selectivity except for a tendency toward mitochondria.

The fluorescence signals produced by peptoids **P1**−**P3** were found to be distributed in the cells' cytoplasm. A trend of these markers to accumulate at the perinuclear region was also identified, as indicated by the arrows (Figure 1). The region close to the nucleus is known to be rich in mitochondria,[32] although no expressive cellular selectivity was noted during the tests of **P1**−**P3**. The cells showed normal morphological aspects (no morphological alteration) as observed by phase contrast microscopy, thus suggesting no cytotoxic effects, in accordance with the MTT experiments.

An interesting study of Vicent and co-workers showed that some peptoid derivatives are co-responsible for effective methods for improving the inhibition of mitochondrion-mediated apoptosis.[31] The subcellular localization of **P1**−**P3** seems to be in accordance with this proposition, especially considering that **P1**−**P3** accumulate close to the cells' nuclei, that is, a region with plenty of mitochondria, although overall **P1**−**P3** were also distributed in the cytoplasm.

Bioimaging experiments conducted with **P4**, however, returned the most interesting results (Figure 2).

P4 showed a distinctive fluorescent pattern, that is, **P4** afforded the most intense fluorescent signal when compared to **P1**−**P3** and accumulated near the cells' nuclei in a sharply defined region (Figure 2, I); i.e., the result is consistent with a mitochondrion-specific stain. No fluorescent staining could be detected inside the cells' nuclei, which were represented as black voids inside the cells. Although the peptoids had dimensions that allowed for passive traffic through nuclear pores, none of the four molecules could be detected inside the cells' nuclei. This result suggests no affinity between the tested peptoids and the components of the nuclei. This result is also in accordance with the importance of an empirically guided optimization, because few modifications afforded huge differences in cellular selectivity.

To ensure the mitochondrial localization of **P4**, co-staining assays were conducted (Figure 2, II) using the commercially available mitochondrial marker known as MitoTracker Red. The experiment confirmed our previous finds that **P4** is selective for mitochondria and an intense purple emission may be noted in the merged images (Figure 2, II-D). These results demonstrate that **P4** has arisen as a new peptoid selective to mitochondria, permeable to the cell membrane with a sharp distribution. Phase contrast images (Figure 2) were also generated to verify the morphological aspects of the cells. Once again, no morphological alterations in MCF-7 cells were observed, as expected and in accordance with the cell viability assays (Figure S3).

Finally, photobleaching experiments were performed to compare the stability performance of **P4** and MitoTracker Red (Figure 3). As noted, **P4** showed a performance superior by far compared with that of the commercial dye (also see Figure S4).

The ROI (regions of interest, seen as yellow rectangles in Figure 3) photobleaching results demonstrated that **P4** was considerably more resistant than MitoTracker Red. **P4** emission fades gradually until the 4 h photobleaching time point. Still, its emission was not extinct after 4 h, the value retaining more than 50% of the fluorescence intensity at the end of the assay (also see Figure S4). The MitoTracker Red ROI analyses showed a gradual fluorescence fading off from 5 to 30 min. Afterward, its fluorescence emission was widely reduced, reaching a very low level at the end of the assay (Figure 3 and Figure S4). The MitoTracker Red fluorescence emission became visually undetectable after the samples had been photobleached for 4 h (Figure 3).

In summary, four new fluorescent peptoids were obtained using the multicomponent Ugi 4CR. These peptoids allowed for cellular studies with precise subcellular localization and dynamic distribution in both live and fixed cells. All peptidomimetics could be tested at the nanomolar scale (10 nM), avoiding any interference in the cellular processes, avoiding any morphological alteration, and without any notable cytotoxic effect. The results pointed to a possible mitochondrial action of these peptidomimetics. **P4** proved to be highly selective for mitochondria, in accordance with the hypothesis of mitochondrial action of other peptoid derivatives.[31] All results described herein thus opened up new avenues with plenty of room for exploration with regard to cellular studies of peptidomimetics, especially for peptoids from the U4CR. For

DOI: 10.1021/acs.joc.6b00034
J. Org. Chem. 2016, 81, 2646−2651

the first time, fluorescent peptoids could be used at nanomolar concentrations to determine their precise subcellular localization, and one of them (**P4**) showed a high affinity for selectively staining mitochondria with a performance by far superior compared to that of the commercial dye (MitoTracker Red).

EXPERIMENTAL SECTION

General. All reagents and solvents are commercially available and have been directly used without any further purification. NMR spectra were recorded on a 14 T instrument using a 5 mm internal diameter probe operating at 600 MHz for ^{1}H and at 150 MHz for ^{13}C. Chemical shifts are expressed in parts per million and referenced to the signals of the residual hydrogen atoms of the deuterated solvent ($CDCl_3$), as indicated in the legends. High-resolution ESI(+)-MS analyses were conducted in a triple TOF with internal calibration and direct solution (1 ppm) infusion.

General Procedure for the Syntheses of P1−P4 (see Scheme 1). To 20 mL of methanol were added 1 mmol of the aldehyde and 1 mmol of benzylamine. The mixture was stirred for 1 h followed by the addition of 1 mmol of the coumarin (acid) derivative and 1 mmol of the isonitrile. The mixture was stirred at room temperature for 72 h, concentrated under vacuum, and purified with a chromatographic column [40:60 (v/v) CH_2Cl_2:AcOEt] to afford **P1−P4**.

P1: obtained in 70% yield (184 mg, amorphous solid); ^{1}H NMR (600 MHz, $CDCl_3$) δ 7.76 (s, 1H), 7.51 (br, 1H), 7.23−7.13 (m, 6H), 7.06−7.00 (m, 5H), 6.53 (dd, 1H, 9.0 and 2.4 Hz), 6.43 (s, 1H), 6.32 (s, 1H), 3.49−3.41 (m, 2H), 3.36 (q, 4H, 7.0 Hz), 1.41−1.38 (m, 2H), 1.17 (t, 6H, 7.0 Hz), 1.67−1.64 (m, 2H), 0.96 (t, 3H, 7.3 Hz); ^{13}C NMR (150 MHz, $CDCl_3$) δ 169.3, 167.1, 159.4, 156.8, 151.5, 143.8, 139.5, 134.5, 130.5, 129.8, 129.6, 128.3,128.1, 127.9, 127.5, 109.5, 97.2, 65.8, 45.0, 39.8, 31.4, 20.2, 13.8, 12.3; mp 193−194 °C; high-resolution ESI(+)-MS calcd for $[C_{32}H_{35}N_3O_4 + H]^+$ 526.2700, found 526.2699; water solubility 0.2 mg mL^{-1}.

P2: obtained in 35% yield (100 mg, amorphous solid); ^{1}H NMR (600 MHz, $CDCl_3$) δ 7.75 (s, 1H), 7.52 (br, 1H), 7.23−7.21 (d, 1H, 12.0 Hz), 7.09−7.00 (m, 5H), 6.70−6.67 (m, 2H), 6.60 (d, 1H, 12.0 Hz), 6.57 (d, 1H, 12.0 Hz), 6.34 (s, 2H), 5.85 (s, 2H), 3.47−3.41 (m, 2H), 3.36 (q, 4H, 7.0 Hz), 1.66−1.61 (m, 2H), 1.45−1.38 (m, 2H), 1.17 (t, 6H, 7.0 Hz), 0.96 (t, 3H, 7.3 Hz); ^{13}C NMR (150 MHz, $CDCl_3$) δ 169.2, 167.0, 159.4, 156.8, 147.3, 147.2, 143.7, 139.4, 129.8, 129.6, 128.4, 128.2, 127.6 124.5, 110.9, 107.8, 101.0, 65.3, 45.1, 39.9, 31.4, 20.2, 13.8, 12.3; mp 200−201 °C; high-resolution ESI(+)-MS calcd for $[C_{33}H_{35}N_3O_6 + H]^+$ 570.2599, found 570.2598; water solubility 0.2 mg mL^{-1}.

P3: obtained in 82% yield (215 mg, amorphous solid); ^{1}H NMR (600 MHz, $CDCl_3$) δ 7.72 (s, 1H), 7.20−7.15 (m, 6H), 7.07−7.00 (m, 6H), 6.52 (dd, 1H, 9.0 and 2.4 Hz), 6.31 (d, 1H, 2.6 Hz), 6.29 (s, 1H), 3.36 (q, 4H, 7.3 Hz), 1.47 (s, 9H), 1.17 (t, 6H, 7.2 Hz); ^{13}C NMR (150 MHz, $CDCl_3$) δ 168.5, 167.0, 159.1, 156.8, 151.4, 143.6, 139.6, 134.7, 130.5, 129.7, 129.6, 128.2, 128.0, 127.8, 127.4, 109.1, 97.0, 66.2, 51.9, 44.8, 28.7, 12.3; mp 209−210 °C; high-resolution ESI(+)-MS calcd for $[C_{32}H_{35}N_3O_4 + H]^+$ 526.2700, found 526.2706; water solubility 0.5 mg mL^{-1}.

P4: obtained in 56% yield (160 mg, amorphous solid); ^{1}H NMR (600 MHz, $CDCl_3$) δ 7.70 (s, 1H), 7.19 (d, 1H, 8.8 Hz), 7.07−7.02 (m, 6H), 6.70−6.67 (m, 2H), 6.60 (d, 1H, 8.8 Hz), 6.52 (dd, 1H, 9.0 and 2.4 Hz), 6.31 (d, 1H, 2.2 Hz), 6.20 (s, 1H), 5.85 (q, 2H, 1.5 Hz), 3.36 (q, 4H, 7.0 Hz), 1.47 (s, 9H), 1.16 (t, 6H, 7.2 Hz); ^{13}C NMR (150 MHz, $CDCl_3$) δ 168.5, 167.0, 159.2, 156.8, 151.5, 147.3, 143.6, 129.7, 128.4, 127.6, 124.5, 117.9, 110.9, 109.2, 107.9, 101.0, 97.0, 65.9, 51.9, 44.9, 28.7, 12.4; mp 227−228 °C; high-resolution ESI(+)-MS calcd for $[C_{33}H_{35}N_3O_6 + H]^+$ 570.2599, found 570.2599; water solubility 0.5 mg mL^{-1}.

ASSOCIATED CONTENT

Supporting Information

The Supporting Information is available free of charge on the ACS Publications website at DOI: 10.1021/acs.joc.6b00034.

NMR spectra, HRMS [ESI(+)-MS], photophysical data, cell viability assays, and cellular experimental procedures (PDF)

AUTHOR INFORMATION

Corresponding Authors

*E-mail: wender@unb.br.

*E-mail: brenno.ipi@gmail.com. Phone: (+) 55 61 31073867.

Notes

The authors declare no competing financial interest.

ACKNOWLEDGMENTS

This work has been supported by CAPES, CNPq, FINEP-MCT, FINATEC, FAPDF, and DPP-UnB. B.A.D.N. also thanks the INCT-Transcend group and LNLS for the use of their facilities.

REFERENCES

(1) Vasco, A. V.; Perez, C. S.; Morales, F. E.; Garay, H. E.; Vasilev, D.; Gavin, J. A.; Wessjohann, L. A.; Rivera, D. G. *J. Org. Chem.* **2015**, *80*, 6697−6707.

(2) Barreto, A. d. F. S.; Vercillo, O. E.; Birkett, M. A.; Caulfield, J. C.; Wessjohann, L. A.; Andrade, C. K. Z. *Org. Biomol. Chem.* **2011**, *9*, 5024−5027.

(3) Bush, J. T.; Walport, L. J.; McGouran, J. F.; Leung, I. K. H.; Berridge, G.; van Berkel, S. S.; Basak, A.; Kessler, B. M.; Schofield, C. J. *Chem. Sci.* **2013**, *4*, 4115−4120.

(4) Vazquez-Romero, A.; Kielland, N.; Arevalo, M. J.; Preciado, S.; Mellanby, R. J.; Feng, Y.; Lavilla, R.; Vendrell, M. *J. Am. Chem. Soc.* **2013**, *135*, 16018−16021.

(5) Salvador, C. E. M.; Pieber, B.; Neu, P. M.; Torvisco, A.; Kleber Z. Andrade, C.; Kappe, C. O. *J. Org. Chem.* **2015**, *80*, 4590−4602.

(6) Brauch, S.; Henze, M.; Osswald, B.; Naumann, K.; Wessjohann, L. A.; van Berkel, S. S.; Westermann, B. *Org. Biomol. Chem.* **2012**, *10*, 958−965.

(7) Rivera, D. G.; Leon, F.; Concepcion, O.; Morales, F. E.; Wessjohann, L. A. *Chem. - Eur. J.* **2013**, *19*, 6417−6428.

(8) Moni, L.; Denissen, M.; Valentini, G.; Mueller, T. J. J.; Riva, R. *Chem. - Eur. J.* **2015**, *21*, 753−762.

(9) Thorp-Greenwood, F. L.; Coogan, M. P.; Mishra, L.; Kumari, N.; Rai, G.; Saripella, S. *New J. Chem.* **2012**, *36*, 64−72.

(10) Nadler, A.; Schultz, C. *Angew. Chem., Int. Ed.* **2013**, *52*, 2408−2410.

(11) Chan, J.; Dodani, S. C.; Chang, C. J. *Nat. Chem.* **2012**, *4*, 973−984.

(12) Neto, B. A. D.; Carvalho, P. H. P. R.; Correa, J. R. *Acc. Chem. Res.* **2015**, *48*, 1560−1569.

(13) Medeiros, G. A.; da Silva, W. A.; Bataglion, G. A.; Ferreira, D. A. C.; de Oliveira, H. C. B.; Eberlin, M. N.; Neto, B. A. D. *Chem. Commun.* **2014**, *50*, 338−340.

(14) Alvim, H. G. O.; Lima, T. B.; de Oliveira, A. L.; de Oliveira, H. C. B.; Silva, F. M.; Gozzo, F. C.; Souza, R. Y.; da Silva, W. A.; Neto, B. A. D. *J. Org. Chem.* **2014**, *79*, 3383−3397.

(15) Ramos, L. M.; Guido, B. C.; Nobrega, C. C.; Corrêa, J. R.; Silva, R. G.; de Oliveira, H. C. B.; Gomes, A. F.; Gozzo, F. C.; Neto, B. A. D. *Chem. - Eur. J.* **2013**, *19*, 4156−4168.

(16) Alvim, H. G. O.; Bataglion, G. A.; Ramos, L. M.; de Oliveira, A. L.; de Oliveira, H. C. B.; Eberlin, M. N.; de Macedo, J. L.; da Silva, W. A.; Neto, B. A. D. *Tetrahedron* **2014**, *70*, 3306−3313.

DOI: 10.1021/acs.joc.6b00034
J. Org. Chem. 2016, 81, 2646−2651

(17) Alvim, H. G. O.; de Lima, T. B.; de Oliveira, H. C. B.; Gozzo, F. C.; de Macedo, J. L.; Abdelnur, P. V.; Silva, W. A.; Neto, B. A. D. *ACS Catal.* **2013**, *3*, 1420−1430.
(18) Alvim, H. G. O.; da Silva Júnior, E. N.; Neto, B. A. D. *RSC Adv.* **2014**, *4*, 54282−54299.
(19) Silva, G. C. O.; Correa, J. R.; Rodrigues, M. O.; Alvim, H. G. O.; Guido, B. C.; Gatto, C. C.; Wanderley, K. A.; Fioramonte, M.; Gozzo, F. C.; de Souza, R.; Neto, B. A. D. *RSC Adv.* **2015**, *5*, 48506−48515.
(20) Dias, G. G.; Rodrigues, B. L.; Resende, J. M.; Calado, H. D. R.; de Simone, C. A.; Silva, V. H. C.; Neto, B. A. D.; Goulart, M. O. F.; Ferreira, F. R.; Meira, A. S.; Pessoa, C.; Correa, J. R.; da Silva Júnior, E. N. *Chem. Commun.* **2015**, *51*, 9141−9144.
(21) D'Angelis do E. S. Barbosa, C.; Corrêa, J. R.; Medeiros, G. A.; Barreto, G.; Magalhães, K. G.; de Oliveira, A. L.; Spencer, J.; Rodrigues, M. O.; Neto, B. A. D. *Chem. - Eur. J.* **2015**, *21*, 5055−5060.
(22) Carvalho, P. H. P. R.; Correa, J. R.; Guido, B. C.; Gatto, C. C.; De Oliveira, H. C. B.; Soares, T. A.; Neto, B. A. D. *Chem. - Eur. J.* **2014**, *20*, 15360−15374.
(23) Neto, B. A. D.; Correa, J. R.; Silva, R. G. *RSC Adv.* **2013**, *3*, 5291−5301.
(24) He, L.; Xu, Q.; Liu, Y.; Wei, H.; Tang, Y.; Lin, W. *ACS Appl. Mater. Interfaces* **2015**, *7*, 12809−12813.
(25) Zhang, X.; Ba, Q.; Gu, Z.; Guo, D.; Zhou, Y.; Xu, Y.; Wang, H.; Ye, D.; Liu, H. *Chem. - Eur. J.* **2015**, *21*, 17415−17421.
(26) Wu, M.-Y.; Li, K.; Liu, Y.-H.; Yu, K.-K.; Xie, Y.-M.; Zhou, X.-D.; Yu, X.-Q. *Biomaterials* **2015**, *53*, 669−678.
(27) Reichardt, C. *Chem. Rev.* **1994**, *94*, 2319−2358.
(28) Ravi, M.; Soujanya, T.; Samanta, A.; Radhakrishnan, T. P. *J. Chem. Soc., Faraday Trans.* **1995**, *91*, 2739−2742.
(29) Corredor, M.; Garrido, M.; Bujons, J.; Orzáez, M.; Perez-Paya, E.; Alfonso, I.; Messeguer, A. *Chem.—Eur. J.* **2015**, *21*, 14122−14128.
(30) Turner, J. P.; Lutz-Rechtin, T.; Moore, K. A.; Rogers, L.; Bhave, O.; Moss, M. A.; Servoss, S. L. *ACS Chem. Neurosci.* **2014**, *5*, 552−558.
(31) Orzáez, M.; Mondragon, L.; Marzo, I.; Sanclimens, G.; Messeguer, A.; Perez-Paya, E.; Vicent, M. J. *Peptides* **2007**, *28*, 958−968.
(32) Glatz, J. F. C.; Luiken, J. J. F. P.; Bonen, A. *Physiol. Rev.* **2010**, *90*, 367−417.

DOI: 10.1021/acs.joc.6b00034
J. Org. Chem. 2016, 81, 2646−2651